Eddy Current Loss in Grain-Oriented Steel Laminations due to Normal Leakage Flux

Wei Wang[1], Arne Nysveen[1], *Senior Member, IEEE*, and Niklas Magnusson[2]

[1]Electric Power Department, Norwegian University of Science and Technology, Trondheim, NO-7491 Norway
[2]SINTEF Energy Research, NO-7465 Trondheim, Norway

Leakage flux penetrating laminated iron cores in power transformers and large generators induces eddy current and local loss. Due to the strong magnetic anisotropy of the lamination structure, the penetrating flux tends to saturate the lamination in its plane, even when the incident stray flux density is low. Therefore, the combined effect of anisotropy and nonlinearity has a great impact on the eddy current distribution and the associated power losses. Moreover, the incident normal flux often interacts with the main flux, where the phase angle between the two fluxes may play a significant role. A measurement device is developed to emulate the actual leakage flux in a steel lamination and the power losses are measured at the flux densities of various magnitudes and phases. The measurement results are compared and interpreted by the results obtained from a finite element analysis, where the homogenization approach for material modelling is implemented, taking the combined effect of magnetic anisotropy and the saturation into account.

Index Terms— **Eddy current, Finite element analysis, Magnetic anisotropy, Power losses, Saturation magnetization.**

I. Introduction

VARIABLE power production and consumption due to e.g. renewable energy sources and charging of electrical vehicles, lead to new load patterns for power apparatuses. In large transformers and generators, the laminated iron cores close to the windings are exposed to leakage flux. The normal leakage flux penetrating the core perpendicularly to the plane of the lamination induces eddy currents and generates power loss [1]. Hence, the core loss can be load dependent and under certain loads, the excessive local loss may lead to hot spots on the core surfaces, and result in deterioration of the core insulation and degradation of the insulating oil.

In the past decades, several experimental works involving normal flux [1]-[2] have been carried out. Those works focus on material characterization under unidirectional flux in a single sheet. However, the actual normal flux is usually superimposed with the main flux. Depending on the loading condition, the phase angle between the two fluxes varies, which may change the induced eddy current distribution and the associated power losses. The research on power loss behavior under flux superimposition is largely lacking, and so far, no experimental investigation has been made on the effect of the phase angle between multidirectional fluxes on the eddy current loss.

The finite element method (FEM) has been widely used in eddy current calculation for decades. To reduce the computational effort several homogenization approaches for modelling laminated cores have been proposed [3]-[5], which enables a direct calculation of classical eddy current and the associated loss in lamination structures. The loss decomposition method [6] allows for calculation of hysteresis loss and excess eddy current loss that have different frequency dependency through a post-processing approach.

The primary aim of this paper is the experimental investigation on the loss influence by the normal flux considering actual leakage flux configuration and the flux superimposition of varying phase angle. The physical interpretation of the effects as well as the theoretical calculation was based on finite element analysis, where the homogenization approach was used to calculate the incremental classical eddy current loss. The hysteresis loss and the excess loss were treated together by a post-processing approach. The obtained measured results were compared with the calculated results.

II. Anisotropic Material Definitions

In classic homogenization scheme [3]-[4], the lamination structure is treated as a single domain, and the permeability and the electrical conductivity of the domain are defined as tensors. The three diagonal components of the permeability tensor differ in a grain-oriented (GO) material (Fig. 1).

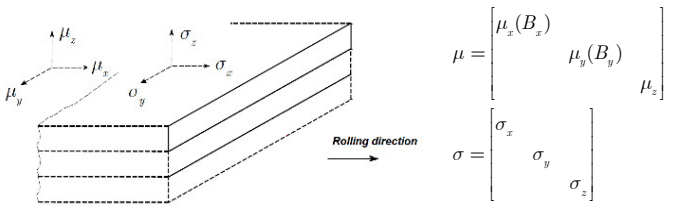

Fig. 1. Illustration of anisotropy of steel lamination. The permeability tensor, μ, and the electrical conductivity tensor, σ, definitions for the lamination of a grain-oriented material.

The effect of the iron-air structure on the permeability in the normal direction, μ_n, is considered by means of a stacking factor γ [4].

$$\frac{1}{\mu_n} = \frac{\gamma}{\mu_f} + \frac{1-\gamma}{\mu_a} \tag{1}$$

where μ_f and μ_a are the permeability of the iron and the air.

Manuscript received November 30, 2020; Corresponding author: Wei Wang (e-mail: weiwan@ntnu.no).
Color versions of one or more of the figures in this paper are available online at http://ieeexplore.ieee.org.
Digital Object Identifier (inserted by IEEE).

The average stacking factor is calculated by:

$$\gamma = \frac{m}{\rho V} \tag{2}$$

where m is the weight of the lamination, V is the volume of the lamination; ρ is the mass density of the steel, 7.65 kg/dm^3. The test lamination is made of cold-rolled GO electrical steel strips (30P120 [7]). The nominal thickness is 0.30 mm with a 10% variation. The calculated stacking factor is 0.97, thus μ_n is approximately 30 according to (1).

To account for the nonlinearity effect, *B-H* curves up to the saturation level are required. At least two *B-H* curves (B_x-H_x curve for B_y=0 and B_y-H_y curve for B_x=0) shall be used for a grain-oriented material. In our test, the two curves were obtained from the single sheet tests (SSTs) in the rolling direction and the transverse direction, respectively. Multiple samples were measured and the permeabilities (mean value) in two orthogonal directions are presented in Fig. 2.

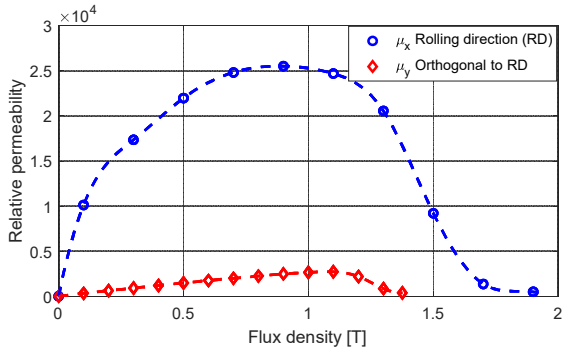

Fig. 2. The components of the permeability tensor versus flux density measured using the single sheet tester (SST). (μ_x: rolling direction; μ_y: orthogonal to rolling direction)

A geometry dependent equivalent electrical conductivity [5] is used in the normal direction.

$$\sigma_n = \left(\frac{\delta}{b}\right)^2 \sigma_f \tag{3}$$

where σ_f is the isotropic conductivity [7] of the GO steels, and δ and b are the thickness and the width of the sheet.

TABLE I
THE PERMEABILITY TENSOR AND THE ELECTRICAL CONDUCTIVITY TENSOR

Relative permeability		Electrical conductivity [S/m]	
μ_x	μ_x *(B)* ref. to Fig. 2	σ_x	2.08×10^6
μ_y	μ_y *(B)* ref. to Fig. 2	σ_y	2.08×10^6
μ_z	30	σ_z	2.08×10^2

III. Experimental Investigation

A. Measurement principles and instrument

To emulate the actual leakage flux configuration in the steel lamination exposed to normal flux, we have developed an instrument for loss measurements under multidirectional flux [8]. In the loss measurement system (Fig. 3), the main flux was generated in a square lamination frame with excitation coils and voltage pick-up coils. The normal direction flux was generated in a C-shaped powder core, in which the flux (with varying magnitude and phase angle) was controlled by the auxiliary excitation coils. The net loss P_{net} in the test specimen is calculated by:

$$P_{net} = P_m + P_m^a - P_{pow} \tag{4}$$

where P_m and P_m^a are the measured power losses from the wattmeter of the main excitation system and the auxiliary excitation system. The measurement reading is obtained with double excitations. The power loss of the C-shaped powder core P_{pow} is calibrated [9] under specified flux densities and frequency prior to fabrication.

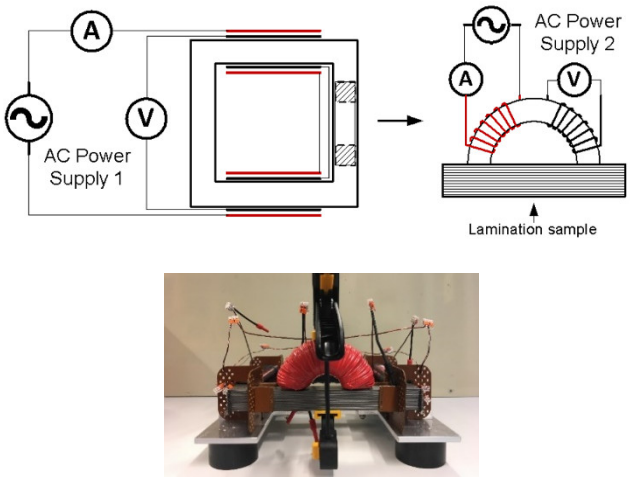

Fig. 3. Loss measurement system with main flux superimposed with leakage flux in the normal direction. The AC power supply 1 connects to the windings wrapping around the square frame and supplies main flux. The AC power supply 2 connects to the winding wrapping around the C-shaped powder core and supplies artificial leakage flux. The C-shaped core is mounted on the surface of the lamination to generate the normal flux. The power source is ITECH IT7627 and the power analyzer is YOKOGAWA WT3000.

B. Measurement under single excitation

The power loss is measured under a single excitation (without main flux in the lamination frame) by the C-shaped powder core. The measurement is performed at 50 and 25 Hz, and the flux density is varied from 0.2 to 0.8 T (Fig. 4). A rapid increase of the power loss with increasing flux density and frequency can be observed.

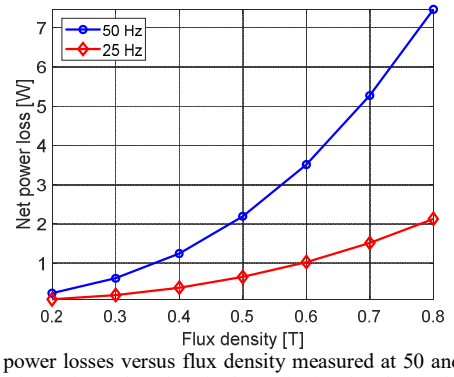

Fig. 4. Net power losses versus flux density measured at 50 and 25 Hz. The measurement is performed under single excitation by the C-shaped powder core.

The loss dependency on flux density B_l and frequency f can be formulated in form of Steinmetz's equation:

$$P \propto f^{1.8} B_l^{2.5} \tag{5}$$

Relation (5) deviates considerably from the classic loss equation where the eddy current loss is proportional to the square of the flux density and square of the frequency.

C. Measurement under multiple excitations

Measurements are performed under multiple excitations with varying phase angle between the main excitation and the auxiliary excitation. The flux density produced in the main frame B_m is set to 1.0 and 1.6 T, whereas the flux density in the C-shaped core B_l is set to 0.2 and 0.4 T. The incremental loss (the difference between the loss measured under superimposed flux and the arithmetic sum of the loss measured with individual excitation systems alone under unidirectional flux) due to flux superimposition are obtained.

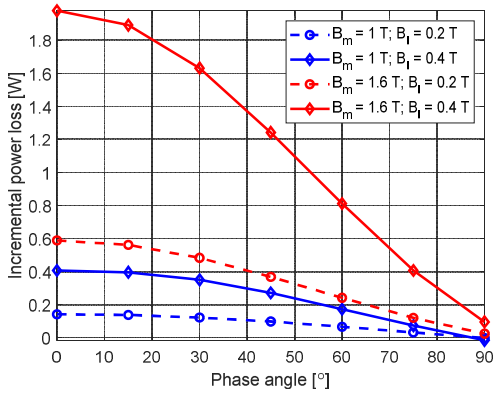

Fig. 5. Incremental power loss versus phase angle measured at different main flux densities B_m combined with different normal leakage flux densities B_l.

As demonstrated in Fig. 5, the power loss increases significantly with increasing flux densities (both the normal flux and the main flux) and with a decreasing phase angle. Apparently, flux superimposition has a greater impact on eddy current loss at a smaller phase angle. In contrast, there is only little discrepancy on loss increase at 90° phase angle.

IV. Finite Element Analysis of Eddy Current Loss

A. Finite element model

A three-dimensional finite element model (Fig. 6) was developed to investigate eddy current loss in the steel lamination under normal flux as well as the effect of the flux superimposition. The homogenization scheme described in Section II was implemented for the GO. The classical eddy current losses were calculated corresponding to the scenarios illustrated in Sections IIIB and IIIC.

The governing equations for the three-dimensional eddy current field in the steel lamination are expressed in terms of a magnetic vector potential and an electric scalar potential ($\vec{A}$, φ-$\vec{A}$ formulation).

$$\nabla \times \left(\left[\mu\right]^{-1} \nabla \times \vec{A} \right) + \left[\sigma\right] \left(\frac{\partial \vec{A}}{\partial t} + \nabla \varphi \right) = 0 \tag{6}$$

$$\nabla \cdot \left\{ -\left[\sigma\right] \left(\frac{\partial \vec{A}}{\partial t} + \nabla \varphi \right) \right\} = 0 \tag{7}$$

where $[\mu]$ and $[\sigma]$ are the tensor of the magnetic permeability and the conductivity, which are defined in Table I.

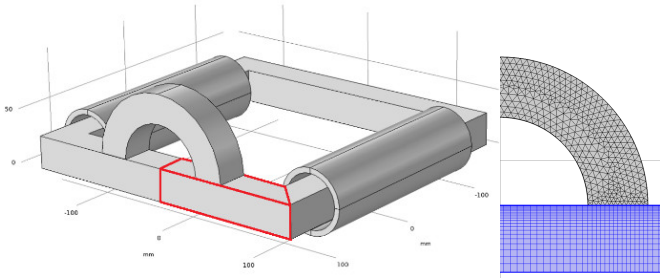

Fig. 6. View of the geometry model and refined mesh in FEM at eddy current concentrated region. In the lamination (blue), the mesh density is growing with geometric sequence towards surface plane. The model was implemented in COMSOL Multiphysics®.

B. Simulation under unidirectional flux

The time-domain simulation was made under the normal flux corresponding to IIB. Figure 7 shows the flux density and the eddy current distribution in the steel lamination at 0.4 T normal flux density. As expected, the majority of the penetrated flux turns to become parallel to the rolling direction and the eddy current induced by the normal flux is constrained within a thin layer (< 3 mm) under the exposure area (interface with C-shaped core).

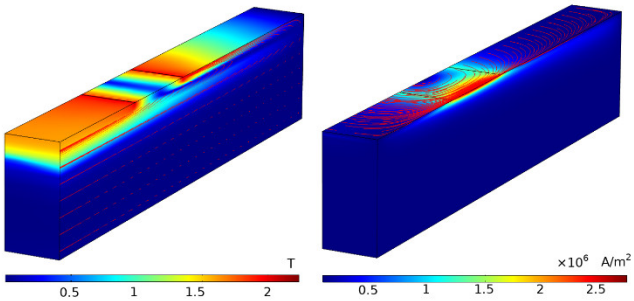

Fig. 7. The flux density (left) and the eddy current (right) distribution in the lamination (a half part of the red region in Fig, 6) at 0.4 T normal flux density. The eddy current is constrained within a thin layer under the exposure area.

The power losses other than the classical eddy current loss are traditionally expressed as hysteresis and excess eddy current loss [6]. The flux density variation in the flux superimposition region influences those losses. We treat these losses together in the post-processing approach. The preserved relationship between this loss and the flux density is obtained from the standardized specific loss measurement [9] performed on the lamination frame.

The simulation result is listed in Table II. To demonstrate the effect of the magnetic nonlinearity, we add linear cases (constant permeability) for comparison to the nonlinear implementation. In the linear simulation, μ_x and μ_y are set to 10000 and 1000, respectively.

TABLE II
POWER LOSS IN THE STEEL LAMINATION DUE TO NORMAL FLUX

Normal flux density [T]	Calculated power loss in the lamination [W]				Measured total losses [W]
	Classical eddy loss P_{e_n} (nonlinear)	Classical eddy loss P_{e_l} (linear)	Hysteresis+ excess eddy loss P_{hex}	Total power loss $P_{e\_n}+P_{hex}$	
0.2	0.18	0.15	0.06	0.24	0.23
0.3	0.53	0.34	0.11	0.64	0.61
0.4	1.07	0.60	0.16	1.23	1.24
0.5	1.99	0.94	0.21	2.20	2.19
0.6	3.21	1.36	0.27	3.48	3.51
0.7	4.82	1.84	0.33	5.15	5.27
0.8	7.06	2.41	0.39	7.45	7.47

The calculated total power loss by the nonlinear implementation have a good agreement with the measurement, whereas the linear approach largely underestimates the eddy current loss, even at very low flux densities. As expected, the classical eddy loss is strictly proportional to the square of the flux density in the linear case. In the nonlinear case, the eddy loss has a flux density dependency of power 2.5 (larger than 2). Thus, the rapid increase of the eddy loss attributes to the flux saturation effect, which largely extends the eddy current region and amplifies the eddy current loss.

C. *Simulation under superimposed multidirectional flux*

The simulation is made under superimposed multidirectional flux corresponding to IIC. Figure 8 demonstrates the development of the eddy current region in the lamination with a varying phase angle. The main flux density and the normal flux density are 1.6 T and 0.2 T, respectively.

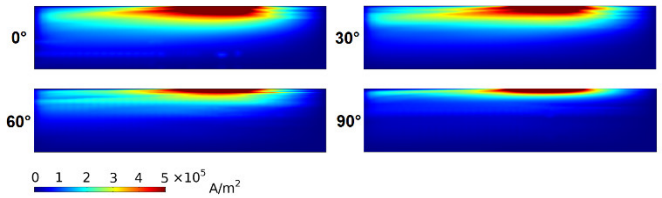

Fig. 8. The maximum eddy current distribution in the lamination under a weak normal flux (0.2 T) superimposed with the main flux (1.6 T) at different phase angles.

The eddy current is more surface concentrated at a larger phase angle (90°), similar to the case without main flux (Fig. 7). In contrast, at a low phase angle, the eddy current region extends deeply due to the saturation effect caused by flux superimposition. The flux superimposition not only expands the classical eddy current loss volume but also enhances the hysteresis loss and excess eddy current losses (Table III).

TABLE III
POWER LOSS DUE TO NORMAL FLUX AND SUPERIMPOSED MAIN FLUX

Phase angle [°]	Calculated power loss in the lamination [W]			Measured total losses [W]
	Classical eddy loss P_e	Hysteresis+excess eddy loss P_{hex}	Total P_e+P_{hex}	
0	0.43	8.90	9.33	9.39
15	0.42	8.87	9.29	9.37
30	0.39	8.84	9.23	9.29
45	0.35	8.81	9.16	9.17
60	0.30	8.76	9.06	9.05
75	0.26	8.73	8.99	8.92
90	0.25	8.66	8.91	8.83

V. CONCLUSIONS

The classical eddy current loss dominates the local power loss of the GO-steel lamination when the lamination is exposed to a normal flux, and the loss increases with the flux density more rapidly than what traditional formula predicts. The anisotropy of the lamination structure makes the penetrated flux saturate easily, thereby expands the eddy current region. When the normal flux is superimposed with a main flux at a low phase angle, the power loss can be further amplified. Hence, the core loss can be locally load dependent.

Power apparatuses such as transformers are often operated and tested (no-load test) close to 90° loading angle. Under inductive loading (i.e., at smaller loading angle), special attention must be paid to the local heat enhancement in the core lamination exposed to the normal leakage flux.

The physical interpretation of the effects shows that the combined effect of anisotropy and nonlinearity must be considered in eddy current loss calculation involving normal flux, even when the flux density is very weak.

ACKNOWLEDGMENT

This work was performed as a part of the project "Thermal Modelling of Transformers" (project number: 255178) funded by the Research Council of Norway, Statnett, Hafslund and Lyse Nett.

REFERENCES

[1] T. Booth, H. Pftzner, "Characteristics of transformer core material for flux normal to the sheet plane," *J. Magn. Magn. Mat*., vol. 133, pp. 183-186, 1994.

[2] N. Hihat, K. Komeza, E. Napieralska Juszczak and J. P. Lecointe, "Experimental and Numerical Characterization of Magnetically Anisotropic Laminations in the Direction Normal to Their Surface," *IEEE Trans. Magn.*, vol. 47, no. 11, pp. 4517-4522, Nov. 2011.

[3] V. C. Silva, G. Meunier and A. Foggia, "A 3-D Finite Element Computation of Eddy Currents and Losses in Laminated Iron Cores Allowing for Electric and Magnetic Anisotropy," *IEEE Trans. Magn.*, vol. 31, pp. 2139 -2141, May 1995.

[4] J. P. A. Bastos and G. Quichaud, "3D modelling of a non-linear anisotropic lamination," *IEEE Trans. Magn.*, vol. 21, no. 6, pp. 2366-2369, November 1985.

[5] J. Wang, H. Lin, Y. Huang and X. Sun, "A New Formulation of Anisotropic Equivalent Conductivity in Laminations," *IEEE Trans. Magn.*, vol. 47, pp. 1378 -1381, 2011.

[6] S. E. Zirkaa, Y. I. Moroza, P. Marketosb and A. J. Moses. "Comparison of engineering methods of loss prediction in thin ferromagnetic laminations," *J. Magn. Magn. Mat*., vol. 20, pp. 2504-2508, 2008.

[7] *Cold-rolled grain-oriented electrical steel strip and sheet delivered in the fully processed state*, Japanese Industrial Standard. JIS C 2553: 2019.

[8] W. Wang, A. Nysveen and N. Magnusson, "Apparatus for loss measurements under multidirectional and dc-bias flux in electrical steel laminations," *Rev. Sci. Instrum*., vol. 91, issue 8, 084705, 2020.

[9] *Magnetic materials - Part 6: Methods of measurement of the magnetic properties of magnetically soft metallic and powder materials at frequencies in the range 20 Hz to 100 kHz by the use of ring specimens*, IEC 60404-6: 2018.